**Research paper**

# The effect of Cu concentration on tensile and compression properties of Ti-10Mo alloy using molecular dynamics simulations

**Aji Abdillah Kharisma[a,b], Haris Rudianto[a,*], Achmad Benny Mutiara [b] and Sulistyo Puspitodjati[b]**

[a]*Department of Mechanical Engineering, Gunadarma University, Depok, West Java, 16431, Indonesia*
[b]*Department of Information Technology, Gunadarma University, Depok, West Java, 16431, Indonesia*

**Abstract**

Titanium alloys have been extensively explored and fabricated for uses in several types of engineering fields. Its superior mechanical properties, Ti-10Mo-xCu alloy has potential applications in hip implants. Determining mechanical qualities via experimental methods takes an admittedly long time, especially when carried out in compression and tensile testing. Therefore, material design modeling using an MD simulation method approach was used to evaluate the mechanical properties on the compression and tensile tests of the Ti-10Mo-xCu alloy. In this research, material design through computer modeling was carried out at 300 K in the x <100> direction of the Ti-10Mo alloy with the addition of Cu composition at 3wt%, 6wt%, 9wt% to evaluate the properties of the alloy. The simulation results of the addition 3wt%, 6wt%, and 9wt% of Cu has produced maximum stresses of 603 MPa, 160 MPa and 236 MPa. The experimental method in the compression test shows a decrease in the maximum stress in the compression test after addition Cu to the Ti-10Mo alloy. It has the same trend value as the compression test outcomes on the experiment and MD simulation method. The result of tensile strengths for the Ti-10Mo-xCu alloy were 7056.8 MPa, 7238.1684 MPa, and 7433.0969 MPa. In short, the addition of copper of 3wt%, 6wt%, 9wt% successfully increased the tensile strength of the prepared titanium alloys. The results of crack propagation in tensile strength by MD simulation were successfully performed based on the increase at high strain until plasticity occurs in the alloy.

# 1. Introduction

For a long time, materials science study has become more popular due to the mechanical properties of metals [1, 2]. A hip fracture is a failure in the upper thighbone. Elderly patients are most commonly affected by hip fractures, when a hip fracture develops in a younger patient, it is frequently the result of a high-energy activity. Hip implants are classified as biomaterials, which are made from metal alloy, polymer, ceramic, and composite, especially titanium alloys [3]. The most popular implant material in biomedical applications is titanium alloy due to its excellent mechanical qualities (such as tensile and compressive strength) [4]. Testing the mechanical properties for hip implants using experimental methods is required for a very long time in the process, especially for testing the mechanical properties of compression tests. Therefore, it is necessary to carry out material design modeling using the molecular dynamic simulation method approach, which can evaluate to obtain faster results from the compression test. The computational method provides a solution for material handling under extreme conditions in the laboratory, such as high temperature and pressure [5]. In 1960, Gibson and Vineyard used MD simulations to investigate radiation damage in Cu [6]. In 1964, Rehman used MD simulations to simulate atomic motion in the liquid argon [7]. In 1967, Verlet solve the classical principles for movement between atoms by implementing the verlet integration [8]. Additionally, research on the molecular dynamics simulations of the Cu/W interface show higher the [1 1 0], [1 1 2] copper yield point and substantially reduced strengths of [1 1 1] copper [9]. Recent investigation, using 2NN MEAM, showed acceptable interatomics for structures Mn-Ni, Co-Fe, Cr-Mn, Co-Cr are constructed [10]. Diffusion bonding at the Mo-Ti interface is critical for bonding composite structures via the temperature effect in MD simulations. When the Ti composition exceeds 50%, the HCP structure is shown to be more stable than the BCC structure [11]. A potential of (Ti1) forming the HCP-BCC transformation to simulate plasticity damage on the HCP Ti property target $\alpha$ (HCP) (Å) is 2.951 [12].

On the other hand, the researchers released various studies on structural aspects, phase transition, crystal growth process, mechanical and magnetic properties on the alloys (such as Cu-Ti [13], Bulk Cu [14], Cubic Cu–Au [15-17], $Ag_{1-x}Au_x$ NiAu, and $Fe_{1-x-y}Ni_xCo_y$ alloys [18-20], when the concentration of Cu increases, the proportion of the crystal structure system changes. Recently, many studies on Ti-based alloys made of various materials have been released via molecular dynamic simulation especially mechanical properties such as compression and tensile test, structural change transformation, (such as Cu/W, Mo/Ti interfaces, Ti-Mo alloys [9, 11], [21, 22], TiAl alloy, $\gamma$-titanium aluminide, TiNi alloy, (TiAl)/$\alpha_2$(Ti$_3$Al) [23-26], single crystal Al [27], TiV alloys [28], copper nanowire [29], Ti-Cu alloy [30]. Nevertheless, as close as we are mindful, none earlier research has been disclosed to describe mechanical behavior and structure evolution of the Ti-10Mo alloys with the addition of 3Cu, 6Cu, and 9Cu were used atomistic scale on the uniaxial tensile and compression loading. The outcome of the research is the modeling of material design of Ti-10Mo-xCu alloys with the output result of mechanical properties of the compression test. The result will be compared with MD simulation and experimental technique. Tensile test modeling with MD simulation is used to forecast stress-strain findings and structural deformation changes that occur without comparing them to experimental results.

## 2. Computational procedure
### 2.1. Interatomic potentials

We adopted the modified embedded atom model (MEAM) provided by M.I. Mendelev [12] to simulate. MEAM defines the asymmetry of the shear variable and the departure of the c/a lattice parameter ratio from the most suitable value, while retaining a linear function. The c/a lattice parameter ratio from suitable value is 1.587 and lattice parameter a = 2.951 on the Ti-Mo lattice that was refined by referring to earlier results from experiments by B.J. Lee [31]. The interatomic potential applied in the Ti-10Mo-xCu alloy is the modified embedded atom method (MEAM) to define various types of

crystal structures such as (FCC, BCC, HCP) among the atoms [23, 31]. The molecular dynamics simulation system employs classical Newtonian laws of motion.

MD simulations containing N particles with the proper positions and momentum vector by denoted $r_i = (x_i, y_i, z_i)$ and $p_i = (p_{i,x}, p_{i,y}, p_{i,z})$. The Hamiltonian (H) of the system [32] is expressed with Eq. (1).

$$H\left(R^N, P^N\right) = \sum_i^N \sum_\alpha \frac{p_i^2, \alpha}{2m_i} + U\left(R^N\right) \qquad (1)$$

Here, $R^N = \{r_1, r_2, ..., r_N\}$ and $P^N = \{p_1, p_2, ... p_N\}$ expressing the initial spatial coordinates and moment forces of all particles in the system. U is the potential energy. The symbol $\alpha$ denotes the three directions (x, y, z), while $m_i$ specifies the mass of the *i* particle.

The systems energy moves each particle in responses to applied forces. The force with the negative indicates the gradient with the Eq. (2). Newton's second Law [32] describes the movement of a particle with the Eq. (3).

$$F_i\left(R^N\right) = -\frac{\partial U\left(R^N\right)}{\partial r_i} \qquad (2)$$

$$m_i \ddot{r}_i = F_i(R^N) \qquad (3)$$

where $F_i$ is system energy with $\ddot{r}_i$ is the second-order derivative of $r_i$ with relation to time. The initial location $R^N$ and the force moment $P^N$ of the particle against time. The total energy ($E_{tot}$) in the system is made of the total potential energy ($E_p$) and kinetic energy ($E_k$) [33], the formula can be obtained in Eqs. (4 and 5).

$$E_{tot} = E_k + E_p \qquad (4)$$

$$E_k = \frac{3}{2} \times N \times k \times T \qquad (5)$$

where, $E_T$ expressed the total energy of the atom group, $E_p$ is the total potential energy of the atom group, and $E_k$ is the total kinetic energy. k is Boltzmann's constant, N is the number of atoms, and T is the temperature of the system.
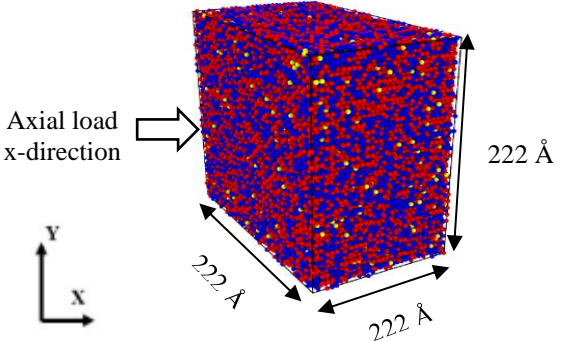
The potential energy that occurs between atoms in an atomic crystal lattice system is known as interatomic potential. In the MEAM, the total energy (E) is expressed by Eq. (6).

$$E = \sum_i^N \left[ F(\bar{\rho}_i) + \frac{1}{2} \sum_{j \neq i} \phi_{ij}(r_{ij}) \right] \qquad (6)$$

In this formula, the embedding energy function (F). $\bar{\rho}_i$ is electron density at the location inhabited by the atom i. The interaction among atoms i and j at a distance of $r_{ij}$ is denoted by $\phi$.

*2.2. Simulation details*

In this work, we used LAMMPS (Large-scale Atomic/Molecular Massively Parallel Simulator) code for materials modeling of Ti-10Mo-xCu alloys were related to mechanical characteristics of the compression and tensile test can be evaluated through by OVITO software [34, 35]. In Fig. 1, the initial configuration of modeling. The units of lattice constant were built using p p p (periodic boundary conditions). The system contains 108000 atoms. The system was set up for equilibrium at room temperature during 10 ps in isothermal-isobaric (NPT) ensemble [36, 37]. The pressure is in (zero pressure) for units metal before conducting a tensile and compression force in the x-direction <100> [38, 39]. Ackland Jones Analysis was used to identify the structural transformations and (CSP) centrosymmetric parameter [40, 41] to identify local crystalline structure of atoms. MD simulations were carried out at 300 K on compression and tension force [39]. The uniaxial deformation quantities of stress to be calculated using Eq. (7). Where, $\sigma$ is stress, F is force and A is cross-sectional area of samples.

$$\sigma = \frac{F}{A} \qquad (7)$$



**Fig. 1.** Initial configuration of modeling. Red, blue, and yellow is represent of titanium, molybdenum, and copper atom, respectively.

**Table 1.** Chemical compositions (wt%).

| Element | Ti | Mo | Cu |
|---|---|---|---|
| Ti-10Mo-3Cu | Balance | 10 | 3 |
| Ti-10Mo-6Cu | Balance | 10 | 6 |
| Ti-10Mo-9Cu | Balance | 10 | 9 |

Based on the existing problem statement shown in Fig. 2, the simulation model results will be validated and verified in order to compare with experimental results. The sample dimensions (in mm) on the compression test used in the experiment method are shown in Fig. 3 for Ti-10Mo-xCu alloys.
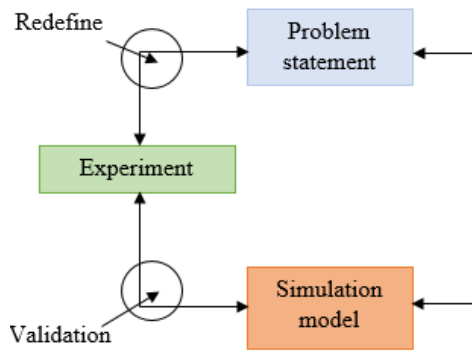


**Fig. 2.** Stages of the research.
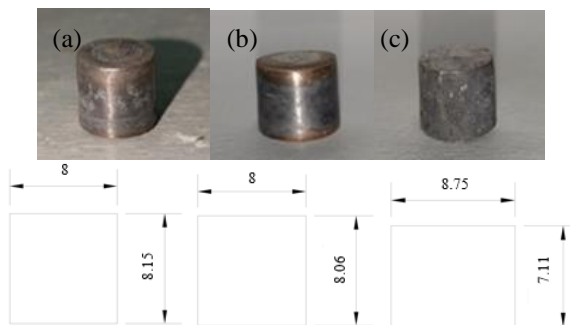


**Fig. 3.** The sample dimensions (experiment method) on the compression test of Ti-10Mo alloys (a)3Cu, (b)6Cu, and (c)9Cu, respectively.

## 3. Results and discussion

*3.1. Stress – strain relation of compression and tensile loading test*

In general, stress-strain relationship curves are used to demonstrate that a material performs under loading situations.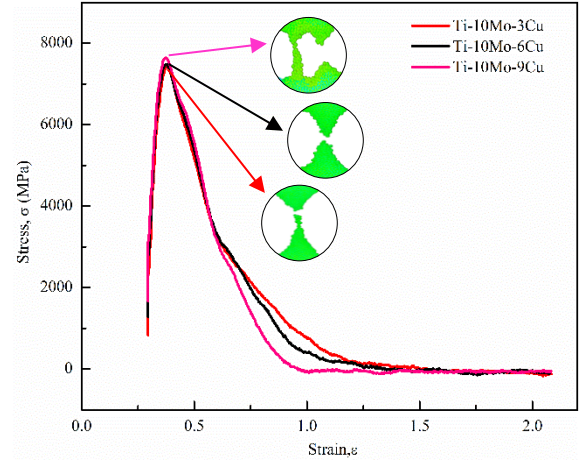 The modulus of elasticity on the maximum compression and tensile qualities of the material can be calculated using the correlation graph of stress and strain [42, 43]. Fig. 4(a) shows, in the <100> x-direction, the result of stress-strain graph for the compression testing on the Ti-10Mo-3Cu element. The Ti-10Mo-3Cu element has a significantly higher peak stress at 300 K than Ti-10Mo-6Cu and Ti-10Mo-9Cu in Fig. 4(b and c). In the Table. 2, the result of compression stress values of Ti-10Mo elements of 3Cu, 6Cu and 9Cu is 603 MPa, 160 MPa and 236 MPa, respectively, which indicate strains during 0.153 0.240, and 0.189 respectively, with the addition of the Cu element to the Ti-10Mo alloy of leading to decrease in stress values. The value of modulus elasticity in the x- direction of compression loading is 4020 MPa, 816 MPa, and 967 MPa, respectively (see Table. 2). This finding is similar to the prior experiments results [24]. The effect of the addition of Cu elements on the maximum stress and modulus elasticity in our results shows a decrease in the Ti-10Mo alloys, consistent with the result of our previous experiments [24]. It contrast [44] have also found that the percentage of when Cu is added produces has been a low modulus of elasticity with the increase of the Cu element [45], this mechanism prevents dislocation movement, hence enhancing the hardness of the Ti-10Mo-xCu alloys.
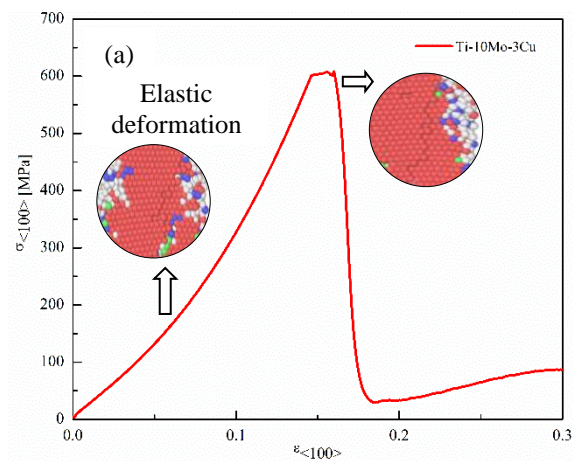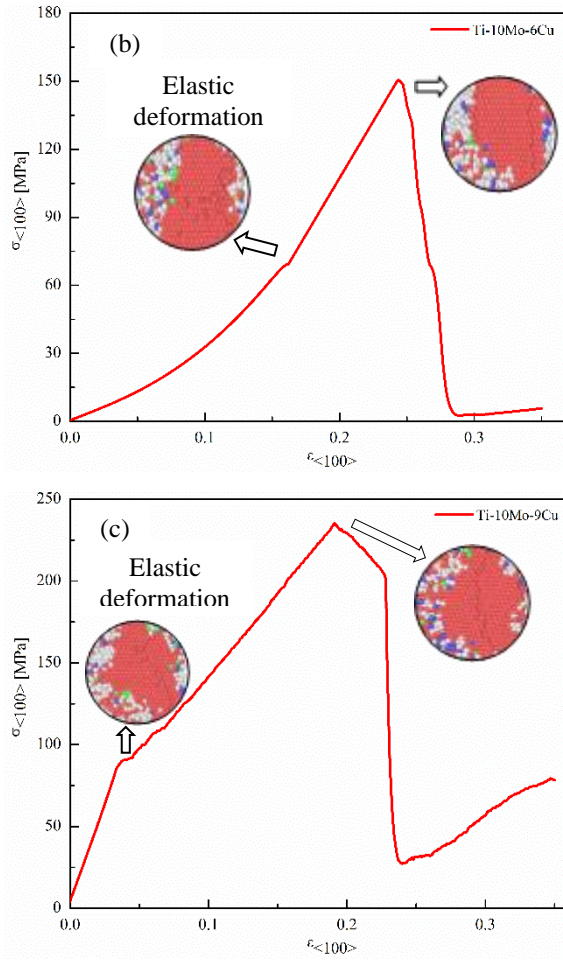
**Fig. 4.** Engineering stress - strain curve for compression tests of titanium alloys with x-direction <100> (a) 3Cu, (b) 6Cu and (c) 9Cu, respectively.

The value maximum stress on the Ti-10Mo-3Cu, Ti-10Mo-6Cu, and Ti-10Mo-9Cu is 7056.8 MPa, 7238.1684 MPa, and 7433.0969 MPa, respectively, with the strain value is 0.355, 0.3562 and 0.37756 are shown in Fig. 5. The highest stress corresponds to the maximal force during stretching that a material meets when strained before breaking, while strain represents the ductility of the material. The increase of the copper percentage can improves the mechanical quality of the Ti-10Mo-xCu alloy for use as a hip implant [46-49]. Our results have teh same trend by Y. Xu et.al [46], yield strength of the Ti-14Cu alloy is increased by 30% and UTS is increased by 25% with the influence of the addition Cu element.



**Fig. 5.** Graph of stress-strain on titanium alloys in tensile test with MD simulation.

**Table. 2.** The modulus elasticity (E), maximum stress ($\sigma_{max}$) on the compression test.

| Properties | Element | $\sigma_{max}$ (MPa) | $\varepsilon$ | E (MPa) |
|---|---|---|---|---|
| | Ti-10Mo-3Cu | 603 | 0.153 | 4020 |
| Compression | Ti-10Mo-6Cu | 160 | 0.240 | 812 |
| | Ti-10Mo-9Cu | 236 | 0.189 | 967 |

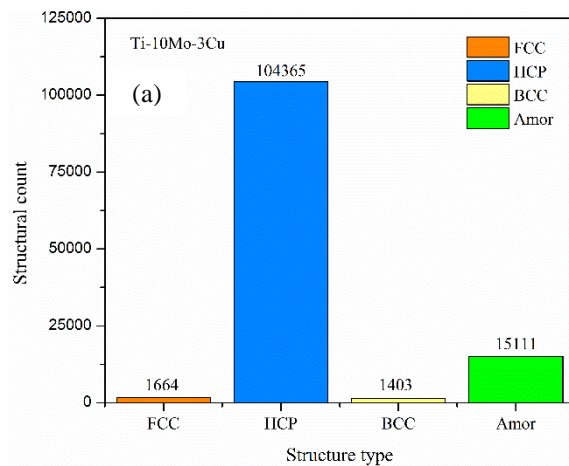### 3.2. Number of structural type units

As illustrated Fig. 6 shows the results of the Ti-10Mo-xCu alloy is defined by four structural type of crystal with HCP (hexagonal close-packed) is green, BCC (body-centered cubic) is orange, FCC (face-centered cubic) is blue, and amorphous (amor) is gray. Fig. 6(a, b and c) shows the number of structural units for Ti-10Mo-xCu alloys on the compression test. The number of HCP lattices in the model was 19503, 12608, and 14780 before stretching of loading at Ti-10Mo-xCu alloy, respectively. In Fig. 6 (a, b and c) shows, the number of structural units produced is 9420 FCC, 58657 HCP, 8526 BCC, and 31140 Amor for Ti-10Mo-3Cu alloy. Ti-10Mo-6Cu alloys produced 8991 FCC, 54347 HCP, 9029 BCC, and Amor 33362. Ti-10Mo-9Cu is 9317 FCC, 56105 HCP, 9192 BCC, and 34887 Amor.
Fig. 7(a, b and c) shows, the number of structural units on the Ti-10Mo-xCu alloys on the tensile test. Ti-10Mo-3Cu has been 1664 FCC, 104365 HCP, 1403 BCC, and Amor 15111. Ti-10Mo-

6Cu was shown by 3528 FCC, 77380 HCP, 8930 BCC, and Amor 31274. Ti-10Mo-9Cu has been 3386 FCC, 77134 HCP, 8559 BCC, and Amor 32218. The number of lattices unchanged as the strain rate is decreased. This is inversely proportional, the fast deformation can be generate a greater proportion of HCP lattice structural change [50]. This is consistent with our simulation results, which are presented in Figs. 6 and 7. The HCP structure number grows as the strain increases. In Figs. 6 and 7, the highest HCP structure type count for tensile and compression is 104365 and 58657 on the Ti-10Mo-3Cu, respectively, indicating that the tensile test has the same condition as the compression test when the increase of strain.

According to structure type count the HCP displayed in Fig. 7, these results have suitable similarities, where the quantity of HCP structure in the compression test result is substantial, namely with the addition of 3Cu, 6Cu and 9Cu in the Ti-10Mo alloy in the compression test at the end of the simulation.
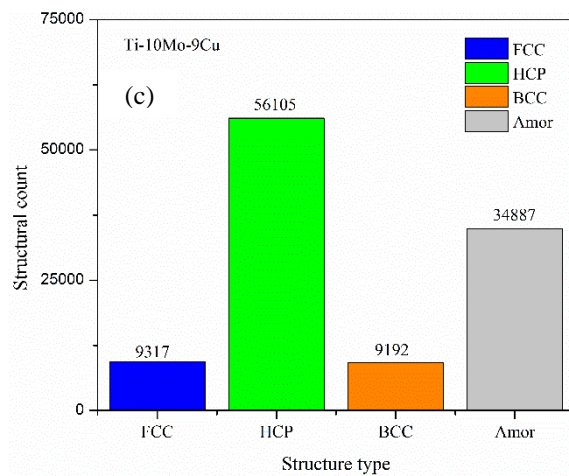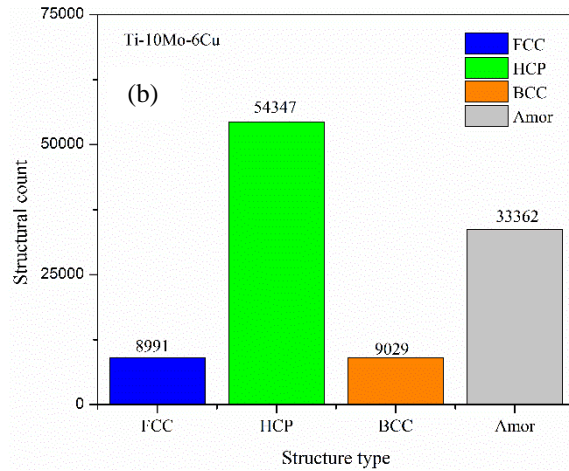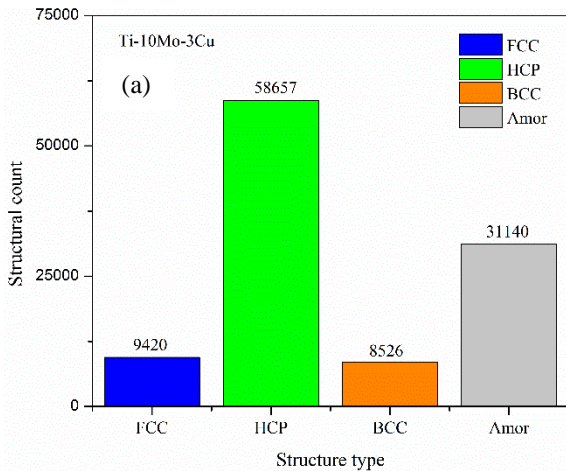






**Fig. 6.** Number of structural type units for Ti-10Mo with addition of copper of compression test, respectively.
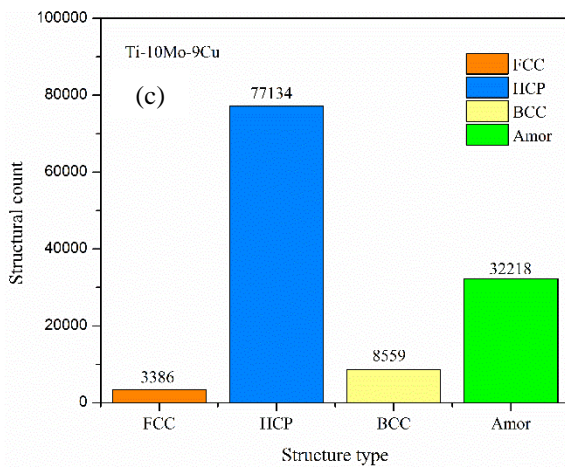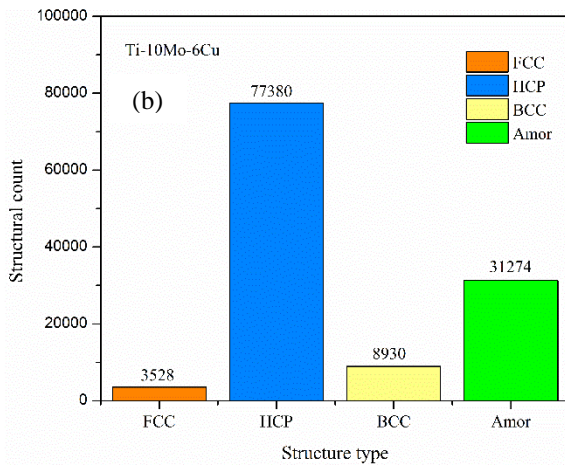
**Fig. 7.** Number of structural type units for Ti-10Mo with addition of copper of tensile test, respectively.

### 3.3. Illustration of structural evolution

In Fig. 8, the centrosymmetric parameter is an important indicator for identifying localized lattice disordered surrounding an atom in solid-state structure, and implemented for identifying when the particles are considered to be bonded by a similar lattice [30]. Red atoms are classified as being in centrosymmetric circumstances, whereas in the simulation box, particles of different colors are classified as being in a non-centrosymmetric condition, implying that a dislocation happened in the atomic structure. The illustration of the respective atomic dislocation mechanisms that occur in Fig. 8(a) displays strain values of 0.074 and 0.153. It is clear that the strain value is very significant when compared to the dislocations that were found in the modeling results as illustrated in Fig. 8(b and c).
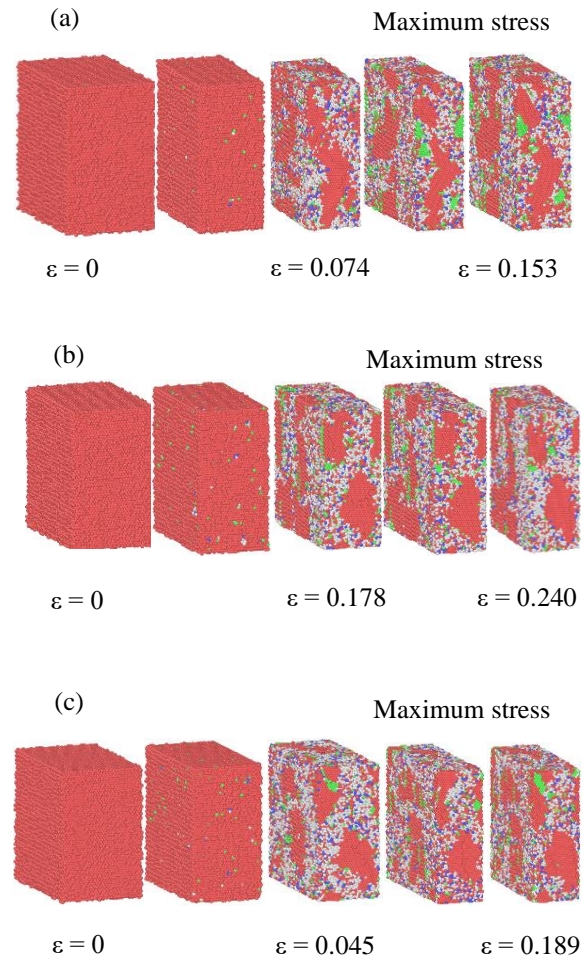


**Fig. 8.** Atom configuration for uniaxial compression loading with centrosymmetric of Ti-10Mo alloy (a) 3Cu, (b) 6Cu, and (c) 9Cu in the <100> direction, respectively.
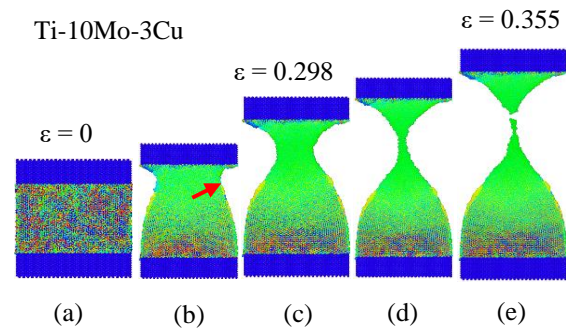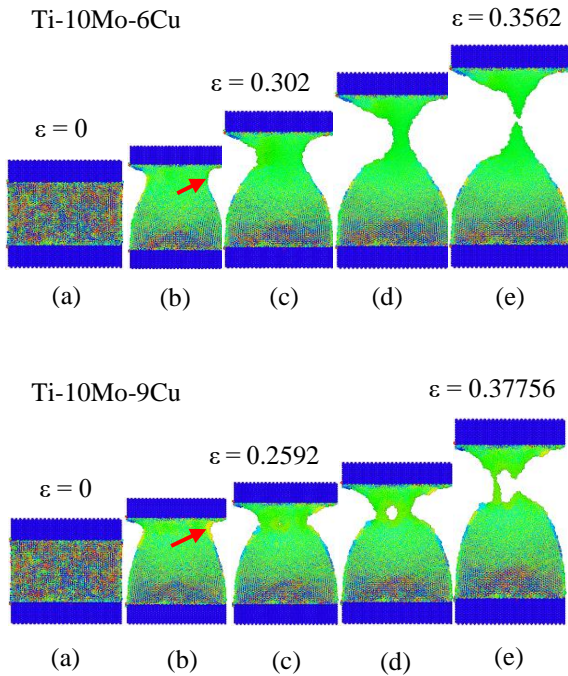
**Fig. 9.** Illustration of atomic configurations of titanium alloys with color coding during 300 K tensile test under the x-direction <100>.

Fig. 9 represents a snapshot of the atomic configuration with a stress tensor in the x-direction that shows the tensile deformation that develops in the Ti-10Mo-xCu alloy at 300 K. Fig. 9(a) shows the regularly organized atoms before relaxing in a state without any pressure applied on the Ti-10Mo-xCu alloy. During the tensile test, several of the initial dislocations (red arrows in Fig. 9(b) started moving to the boundaries and stack to that location, caused by the high energy of grain boundaries [51]. The considerable differences in grain boundary structures was noticed following peak loading. This phenomenon was caused by more frequent grain boundary slips at high strain values [52] with the value of strain is 0.298, 0.3102, and 0.2592 on the Ti-10Mo-xCu alloys (see in Fig. 9(c). As a result, the initial dislocation moves away from the free surface and propagates until it reaches a slip stage. Referring to the graph as illustrated Fig. 5, the plasticity deformed mechanism occurs continuously with increasing strain value. Fig. 9(d), illustrates the atomic necks found in the Ti-10Mo-xCu alloy structure as a result of pressure load which continues to

increase towards ultimate strength on the atom structure. Ultimately, the plastic deformation have been generates with occurs shearing crack on the neck in atomic structure of Ti-10Mo-xCu alloys as illustrated in Fig. 9(e) with strains value is 0.355, 0.3562, and 0.37756 on the Ti-10Mo alloys with the addition of 3Cu, 6Cu, and 9Cu.

*3.4. Radial distribution function of titanium alloys*

The RDF of Ti-10Mo-xCu alloy during compression and tensile stress are shown in Figs. 10 and 11 in the <100> direction. Fig. 10(a and b) displays the Ti-10Mo-3Cu and Ti-10Mo-6Cu have the sharpest peaks in the MoMo pair at the moment of tensile loading, with strain values of 0.355 and 0.362, respectively (at maximum stress), and the highest peak in Fig. 10(c). 9Cu is discovered at TiTi pair having a strain of 0.37756 (at ultimate strength). The sharpest peaks in pictures Figs. 10 and 11 demonstrate that the Ti, Mo, and Cu atom pairs have strong and constant bonding contacts with the surface on the uniaxial tensile and compression loading. The result that follows was made because the Ti, Mo, and Cu atoms were in separate regions, consequently the distance between them extended being under a tensile force.

**Table. 3(a)** Length of links (r, Å) for Ti-10Mo-xCu alloy of the compression test.

| Element | $r_{Ti\text{-}Ti}$ | $r_{Ti\text{-}Mo}$ | $r_{Ti\text{-}Cu}$ | $r_{Mo\text{-}Cu}$ |
|---|---|---|---|---|
| Ti-10Mo-3Cu | 2.6 | 2.7 | 2.68 | 2.55 |
| Ti-10Mo-6Cu | 2.59 | 2.72 | 2.75 | 2.6 |
| Ti-10Mo-9Cu | 2.73 | 2.83 | 2.77 | 2.62 |

**Table. 3(b)** Height peak g(r) for Ti-10Mo-xCu alloy of the compression test.

| Element | Ti-Ti | Ti-Mo | Ti-Cu | Mo-Cu |
|---|---|---|---|---|
| Ti-10Mo-3Cu | 5.08 | 4.12 | 3.97 | 4.1 |
| Ti-10Mo-6Cu | 5.15 | 4.27 | 4.35 | 4.2 |
| Ti-10Mo-9Cu | 5.25 | 3.97 | 4.50 | 4.35 |

**Table. 4(a)** Length of links (r,Å) for Ti-10Mo-xCu alloy of the tensile test.

| Element | $r_{Ti\text{-}Ti}$ | $r_{Ti\text{-}Mo}$ | $r_{Ti\text{-}Cu}$ | $r_{Mo\text{-}Cu}$ |
|---------|------|------|------|------|
| Ti-10Mo-3Cu | 28.5 | 25.7 | 26.6 | 25 |
| Ti-10Mo-6Cu | 29.5 | 26.2 | 27.5 | 25.4 |
| Ti-10Mo-9Cu | 29.9 | 27.3 | 27.7 | 26.5 |

**Table. 4(b)** Height peak g(r) for Ti-10Mo-xCu alloy of the tensile test.

| Element | Ti-Ti | Ti-Mo | Ti-Cu | Mo-Cu |
|---------|-------|-------|-------|-------|
| Ti-10Mo-3Cu | 5.0 | 4.03 | 4.8 | 3.9 |
| Ti-10Mo-6Cu | 5.12 | 4.17 | 4.95 | 3.96 |
| Ti-10Mo-9Cu | 5.20 | 4.0 | 5.15 | 4.14 |
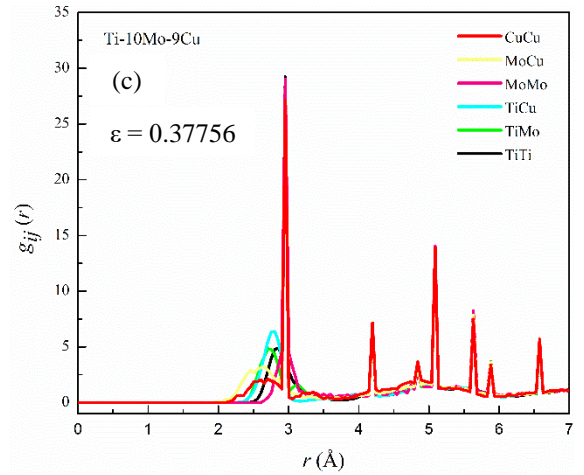


**Fig. 10.** Partial rdf $g_{ij}$ for tensile (a) 3Cu, (b) 6Cu, and (c) 9Cu on titanium alloy in the x-direction, with black, purple, yellow, green, blue and red lines depicted of the TiTi, MoMo, MoCu, TiMo, TiCu, and CuCu pairs, respectively.
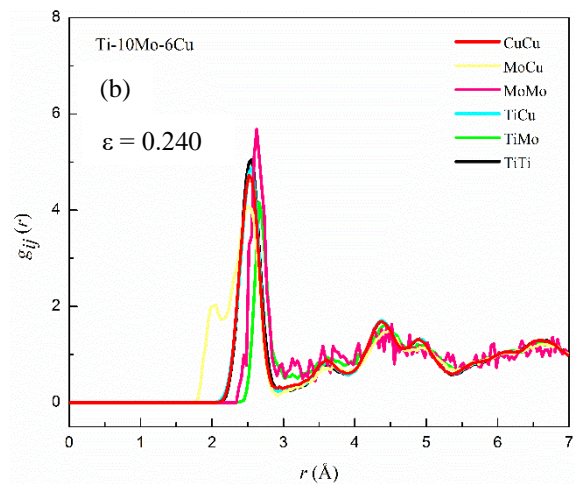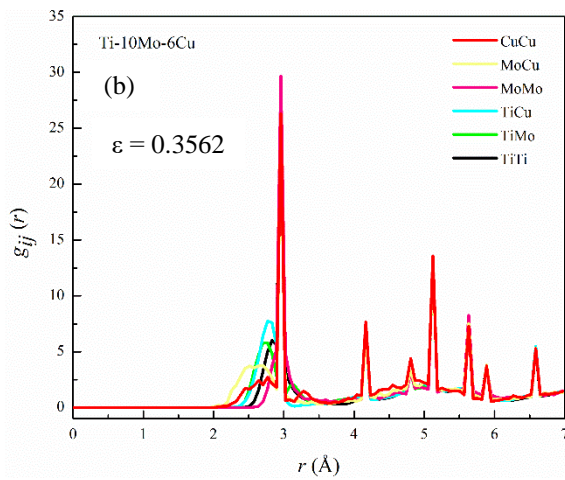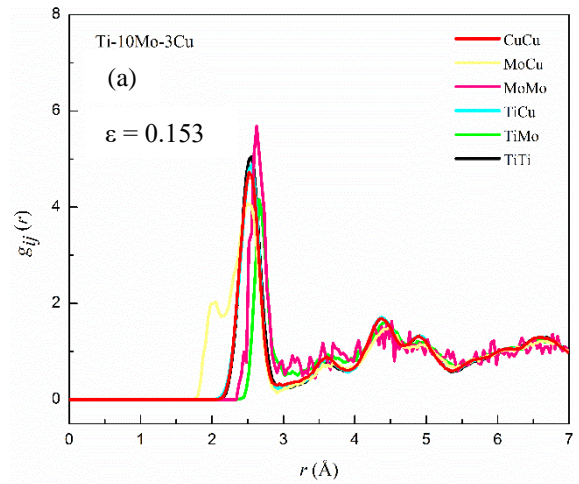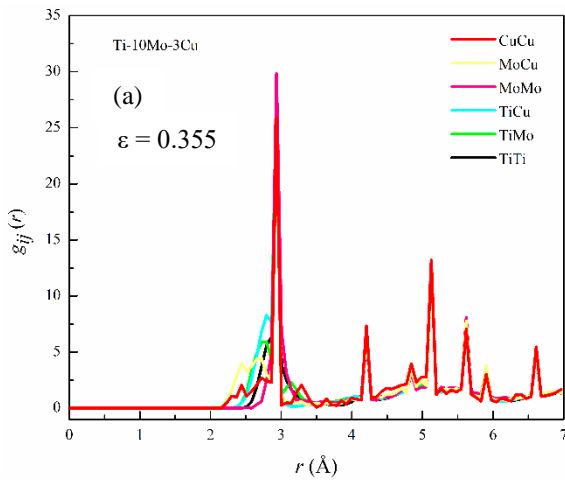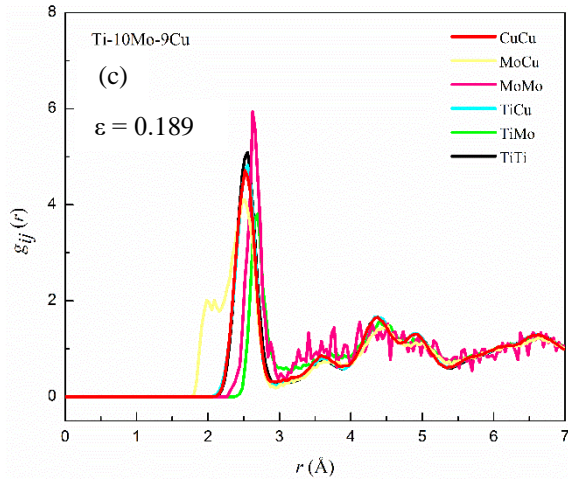
**Fig. 11.** Partial rdf $g_{ij}$ for compression (a) 3Cu, (b) 6Cu, and (c) 9Cu on titanium alloy in the x-direction, with black, green, blue, purple, yellow, and red lines depicted of the TiTi, TiMo, TiCu, MoMo, MoCu, and CuCu pairs, respectively.



**Fig. 12.** Atomic potential energy vs timestep graph under different Ti-10Mo-xCu alloys of compression test.

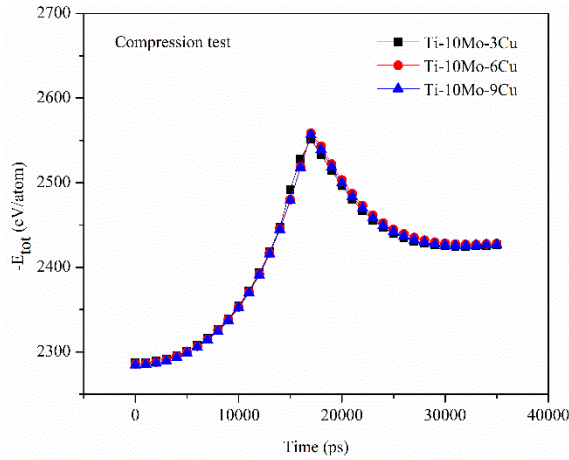The data found reveal that as the timestep increases corresponding with the pressure, $E_{tot}$ always increases continuously. Copper (Cu) is a conductive metal with excellent thermal properties. The effect of Cu doping on the titanium alloy can provide optimal electrical properties. Copper doping can reduce surface area and band gap energy of titanium [53]. The obtained results show that when timestep increased from 0 to 17000 for all the Ti-10Mo-xCu alloys of the compression test, the $E_{tot}$ increase from $E_{tot}$ = 0 eV to $E_{tot}$ Ti-10Mo-3Cu,

6Cu, and 9Cu = −2550 eV, -2570 eV, and 2580 eV, respectively. The $r_{ij}$ increased of rTi-Mo, rTi-Cu, rMo-Cu and the $g_{ij}(r)$ increased from all g(r) of rTi-Mo, rTi-Cu, rMo-Cu on the Ti-10Mo-xCu alloys of compression test and tensile test (see Table. 3(a),(b) and Table. 4(a),(b).
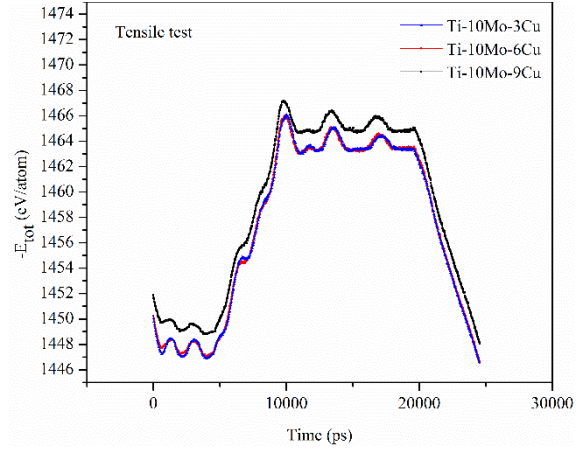


**Fig. 13.** Atomic potential energy vs timestep graph under different Ti-10Mo-xCu alloys of tensile test.

The relationship between the $E_{tot}$ and timestep is shown in Fig. 12. In the tensile test from Fig. 13 shows, the $E_{tot}$ increase from $E_{tot}$ = 0 eV to $E_{tot}$Ti-10Mo-3Cu,6Cu, and 9Cu = −1466 eV, -1466.75 eV, and -1467 eV, respectively. The influence of pressure (loading) parameters is determined by the electronic structure, such as conductivity and resistivity. The density or volume of the alloy decreases as the pressure increases with the time step. It can increased the electrical resistance value and generate superior electronic properties [54, 55].

*3.5. Validation of the titanium alloys modeling between simulation and experiment method*

The validation of the Ti-10Mo-xCu design model in the compression test is shown in Fig. 14 with the size of lattice length of HCP in the simulation model is 220 Å. In HCP, where c is 0.460 nm, a = 0.282 nm [56]. The size of the simulation box on the simulation model of the compression test is (30 × 30 × 30). The value lattice length from the calculation is :
c = 0.460 nm × 30 = 13.8 nm = 138 Å
a = 0.280 nm x 30 = 8.4 nm = 84 Å.

The total of lattice length (c+a) is 222 Å. The volume of the titanium alloy of the MD simulation model must be determined in order to compare the results with the sample size used in the experiment for generating validation output. The volume of HCP can be calculated :

$a = 2r$, so finding the value of, $r = \frac{a}{2}$

$r = \frac{0.88 \text{ mm}}{2} = 0.44$ mm, so $a = 2 \times 0.44$ mm$= 0.88$ mm and c is $1.633 \times a = 1.633 \times 0.88$ mm $= 1.437$ mm. The value of volume HCP Ti alloys is 9.8 mm and can be calculated are shown in Eq. (8).

$$\text{Volume HCP} = 6 \times \frac{a^2\sqrt{3}}{4} \times C \qquad (8)$$
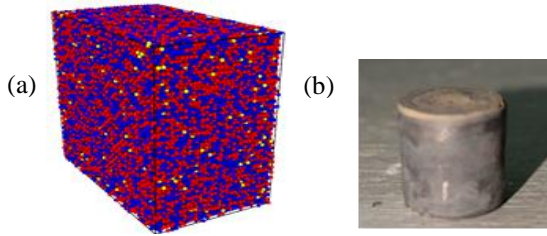


**Fig. 14.** (a) MD simulation model and (b) experimental sample.

Fig. 14(a) shows the result of the MD simulation model, to adjust in Fig. 14(b) the experimental sample. The compression test sample size used in the experimental method is 10 mm and the HCP volume in Ti alloy is 9.8 mm very close to the size value from the other. From Fig. 14, the molecular dynamic simulation generates a lower value, which is consistent with the experimental results [16]. Fig. 15 shows the effect of the addition Cu element will be the decrease of a maximum stress on the MD simulation and experimental method on the compression test. The maximum stress decreases from 603 to 160 MPa in alloys with 3Cu and 6Cu. The stress on 9Cu increases from 160 to 236 MPa.
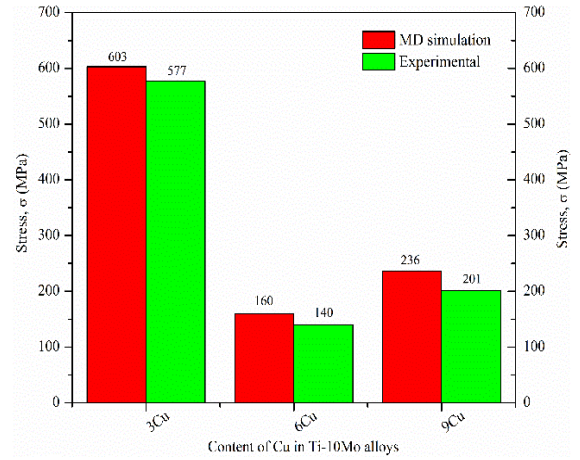


**Fig. 15.** Graph of the comparison results of the stress values in experimental and simulation on the titanium alloys for compression test.

## 4. Conclusions

In this study, the effects of Cu doping on the composition, crystal structure, and mechanical properties of Ti-10Mo-xCu were investigated by MD simulation on the compression and tensile test. The main conclusions are drawn as follows:

1. The maximum stress value of Ti-10Mo-3Cu, Ti-10Mo-6Cu and Ti-10Mo-9Cu alloy on the compression test is 603 MPa, 160 MPa, and 236 MPa, respectively. The highest stress value of 603 MPa which occurs on the Ti-10Mo-3Cu alloy. The effect of the addition Cu element will decrease a maximum stress on the MD simulation and experimental method.

2. On the tensile test results, the stress values at Ti-10Mo alloys with 3wt%, 6wt%, and 9wt% of Cu were then determined to be 7056.8 MPa, 7238.1684 MPa, and 7433.0969 MPa, respectively, with strain values of 0.355, 0.3562 and 0.37756. The highest stress value of 7433.0969 MPa which occurs on the Ti-10Mo-9Cu alloy.

3. Molecular dynamics simulation reveals that Ti-10Mo-xCu alloys with cracks rapidly lose stability when subjected to compression and tensile loads. The crack propagation results in the MD compression and tensile simulation were successfully performed based on the increase at high strain with the resulting structural change, the number of structural units and mechanical deformation.

# References

[1] X. Li, L. Lu, X. Zhang and H. Gao, "Mechanical properties and deformation mechanisms of gradient nanostructured metals and alloys", *Nat Rev Mater.,* Vol. 5, No. 9, pp. 706-723, (2020).

[2] T.O. Olugbade and J. Lu, "Literature review on the mechanical properties of materials after surface mechanical attrition treatment (SMAT)", *NMS.,* Vol. 2, No. 1, pp. 3-31, (2020).

[3] D.F. Williams, "Definitions in biomaterial", *J. Polym. Sci., Part C:Polym. Lett.,* Vol. 26, No. 9, pp. 414-414, (1988).

[4] M. Saini, Y. Singh, P. Arora, V. Arora and K. Jain, "Implant biomaterials: A comprehensive review"., *WJCC,* Vol. 3, No. 1, pp. 52-57, (2015).

[5] J.G. Lee, *Computational materials science an introduction,* 2$^{nd}$ ed., CRC Press, New York, (2016).

[6] Z.D. Sha, W.H. Wong, Q. Pei, P.S. Branicio, L. Zishun, T. Wang, T. Guo adn H. Gao, "Atomistic origin of size effects in fatigue behavior of metallic glasses", *J Mech Phys Solids.,* Vol. 104, No. 7, pp. 84-95, (2017).

[7] M.R. Akbarpour, H.M. Mirabad, A. Hemmati and H.S. Kim, "Processing and microstructure of Ti-Cu binary alloys: A comprehensive review", *Prog. Mater. Sci.,* Vol. 127, No. 6, pp. 3306, (2022).

[8] L. Verlet, "Computer experiment on classical fluids, I. Thermodynamical properties of lennard-jones molecules", *Phys. Rev.,* Vol. 159, No. 1, pp. 98-103, (1967).

[9] G.C. Ma, J.L. Fan and H.R. Gong, "Mechanical behavior of Cu-W interface systems upon tensile loading from molecular dynamics simulations", *Comput. Mater. Sci.,* Vol. 152, No. 9, pp. 165-168, (2018).

[10] W.M. Choi, Y. Kim, D. Seol and B.J. Lee, "Modified embedded-atom method interatomic potentials for the Co-Cr, Co-Fe, Co-Mn, Cr-Mn and Mn-Ni binary systems", *Comput. Mater. Sci.,* Vol. 130, No. 4, pp. 121-129, (2017).

[11] M. Luo, L. Liang, L. Lang, S. Xiao, W. Hu and H. Deng, "Molecular dynamics simulations of the characteristics of Mo/Ti interfaces", *Comput. Mater. Sci.,* Vol. 141, No. 1, pp. 293-301, (2018).

[12] G.J. Ackland, M.I. Mendelev and T.L. Underwood, "Development of an interatomic potential for the simulation of defects, plasticity and phase transformations in titanium", *J. Chem. Phys.,* Vol. 145, No. 10, pp. 1-33, (2016).

[13] V. Fotopoulos, C.S. O'Hern, M.D. Shattuck and A.L. Shluger, "Modeling the effects of varying the Ti concentration on the mechanical properties of Cu-Ti alloys", *ACS Omega.,* Vol. 9, No. 9, pp. 10286-10298, (2024).

[14] D.N. Trong, V.C. Long and S. Țălu, "Molecular dynamics simulation of bulk Cu material under various factors",

*Appl. Sci.*, Vol. 12, No. 9, pp. 4437, (2022).

[15]    T.T. Quoc, V.C. Long, S. Ţălu and D.N. Trong, "Molecular Dynamics Study on the Crystallization Process of Cubic Cu–Au Alloy", *Appl. Sci.*, Vol. 12, No. 1, pp. 946, (2022).

[16]    A. A. Kharisma, H. Rudianto, A.B. Mutiara, S. Puspitodjati, F.H. Latief, W.A. Sukarto, W.B. Widyatno, D. Aryanto and C. Firdharini, "The effects of copper on the mechanical properties of Ti-10Mo alloy prepared by powder metallurgy method", *J Met Mater Miner.*, Vol. 34, No. 1, pp. 1813, (2024).

[17]    D.N. Trong, V.C. Long, U. Saraç, V.D. Quoc and S. Ţălu, "First-principles calculations of crystallographic and electronic structural properties of Au-Cu alloys", *J. Compos. Sci.*, Vol. 6, No. 12, pp. 383-394, (2022).

[18]    T.T. Quoc, P.N. Dang, D.N. Trong, V.C. Long and Ş. Ţălu, "Molecular dynamics study influence of factors on the structure, phase transition, and crystallization of the $Ag_{1-x}Au_x$, x = 0.25, 0.5, 0.75 alloy", *Mater. Today Commun.*, Vol. 37, No. 2, pp. 107119, (2023).

[19]    DN. Trong, V.C. Long and S. Ţălu, "The structure and crystallizing process of NiAu alloy: a molecular dynamics simulation method", *J. Compos. Sci.,* Vol. 5, No. 1, pp. 18-32, (2021).

[20]    D.N. Trong, V.C. Long and S. Ţălu, "Effects of number of atoms and doping concentration on the structure, phase transition, and crystallization process of $Fe_{1-x-y}Ni_xCo_y$ alloy: A molecular dynamic study", *Appl. Sci.*, Vol. 12, No. 17, pp. 8473, (2022).

[21]    O. Ashkani, M.R. Tavighi, M. Karamimoghadam, M. Moradi, M. Bodaghi and M. Rezayat, "Influence of aluminum and copper on mechanical properties of biocompatible Ti-Mo alloys: A simulation-based investigation", *Micromachines.,* Vol. 14. No. 5, pp. 1081-1094, (2023).

[22]    Z. Gao, H. Luo, Q. Li and Y. Wan, "Preparation and characterization of Ti-10Mo alloy by mechanical alloying," *Metallogr. Microstruct. Anal.,* Vol. 1, pp. 282-289, (2012).

[23]    R. Arifin, F. Astuti, M.A. Baqiya, Y. Winardi, Y.A. Wicaksono, Darminto and A. Selamat, "Structural change of TiAl alloy under uniaxial tension and compression in the <001> direction : A molecular dynamics study", *MDPI : Metals.,* Vol. 11, No. 11, pp. 1-14, (2021).

[24]    R. Arifin, D.R.P. Setiawan, D. Triawan, A.F.S. Putra, Munaji, Y. Winardi, W.T. Putra and Darminto, "Structural transformation of Ti-based alloys during tensile and compressive loading: An insight from molecular dynamics simulations", *MRS Commun.*, Vol. 13, No. 2, pp. 225-232, (2023).

[25]    J. Liu and L. Zhang, "Molecular dynamics simulation of the tensile deformation behavior of the $\gamma(TiAl)/\alpha_2(Ti_3Al)$ interface at different temperatures", *J. Mater. Eng. Perform.,* Vol. 31, No. 2, pp. 918-932, (2022).

[26]    H. Ganesan, I. Scheider and C.J. Cryon, "Quantifying the high-temperature separation behavior of lamellar interfaces in γ-titanium aluminide under tensile loading by molecular dynamics", *Comput. Mater. Sci.,* Vol. 7, No. 7 pp. 1-17, (2020).

[27]    Z. Li, Y. Gao, S. Zhan, H. Fang and Z. Zhang, "Molecular dynamics study on temperature and strain rate depedences of mechanical properties of single crystal Al under uniaxial loading", *AIP Advances.,* Vol. 10, No. 7, pp. 1-15, (2020).

[28]    W.L. Zhou, Y. Liu, B.Y. Wang, Y. Song, C.N. Niu and S. Hu, "Molecular dynamics calculations of stability and phase transformation of TiV alloy under uniaxial tensile test", *Mater. Res. Express.,* Vol. 8. No. 6, pp. 1-13, (2021).

[29]    L. Zhao and Y. Liu, "The influence mechanism of the strain rate on the tensile behavior of copper nanowire",

*Sci. China Technol. Sci.,* Vol. 62, No. 11, pp. 2014-2019, (2019).

[30] S.C. Tao, J.L. Xu, L. Yuan, J.M. Luo and Y.F. Zheng, "Microstructure, mechanical properties and antibacterial properties of the microwave sintered porous Ti-3Cu alloy," *J. Alloys Compd.,* Vol. 812, No. pp. 152142, (2020).

[31] J. Wang, S.H. Oh and B.J. Lee, "Second-nearest-neighbor modified embedded-atom method interatomic potential for Cu-M (M=Co,Mo) binary systems", *Comput. Mater. Sci.,* Vol. 178, No. 1, pp. 1-6, (2020).

[32] K. Zhou and B. Liu, *Molecular Dynamics Simulation Fundamentals And Applications*, 1st ed., Elsevier, United Kingdom, pp. 5-6, (2022).

[33] S.T. Oyinbo and T.C. Jen, "Molecular dynamics investigation of temperature effect and surface configurations on multiple impacts plastic deformation in a palladium-copper composite metal membrane (CMM): A cold gas dynamic spray (CGDS) process", *Comput. Mater. Sci*., Vol. 185, pp. 109968, (2020).

[34] K. Nordlund, *Introduction to molecular dynamics,* University of Helsinki, Finland, pp. 65, (2015).

[35] Plimpton and J. Steven, "*LAMMPS and classical molecular dynamics for materials modeling". Conference: Proposed for presentation at the OLCF",* United States, pp. 6-12, (2015).

[36] S. Nose, "A molecular dynamics method for simulations in the canonical ensemble", *Mol. Phys.,* Vol. 52, No. 2, pp. 255-268, (1984).

[37] W.G. Hoover, "Canonical dynamics: Equilibrium phase-space distributions", *Phys. Rev. A.,* Vol. 31, No. 3, pp. 1695-1697, (1985).

[38] M.A. Tschopp, D.E. Spearot and D.L. McDowell, "Atomistic simulations of homogeneous dislocation nucleation in single crystal copper", *Model. Simul. Mater. Sci. Eng*., Vol. 15, No. 7, pp. 693-710, (2007).

[39] M.A. Tschopp and D.L. McDowell, "Influence of single crystal orientation on homogeneous dislocation nucleation under uniaxial loading", *J Mech Phys Solids*., Vol. 56, No. 5, pp. 1806–1830, (2008).

[40] G.J. Ackland and A.P. Jones, "Applications of local crystal structure measures in experiment and simulation", *Phys. Rev. B.,* Vol. 73, No. 5, pp. 0541041-054111, (2006).

[41] C.L. Kelchner, S.J. Plimpton and J.C. Hamilton, "Dislocation nucleation and defect structure during surface indentation", *Phys. Rev. B.,* Vol. 58, No. 17, pp. 11085-11088, (1998).

[42] J. Wang, Z. Ren, S. Yang, J. Ning, S. Zhang and Y. Bian, "The influence of the strain rate and prestatic stress on the dynamic mechanical properties of sandstone- A case study from china", *Materials.,* Vol. 16, No. 9, pp. 3591-3605, (2023).

[43] N. Abbasnezhad, A. Khavandi, J. Fitoussi, H. Arabi, M. Shirinbayan and A. Tcharkhtchi, "Influence of loading conditions on the overall mechanical behavior of polyether-ether-ketone (PEEK)", *Int. J. Fatigue.,* Vol. 109, No. 4, pp. 83-92, (2018).

[44] X. Mao, A. Shi, R. Wang, J. Nie, G. Qin, D. Chen and E. Zhang, "The influence of copper content on the elastic modulus and antibacterial properties of Ti-13Nb-13Zr-xCu alloys", *MDPI : Metals,* Vol. 12, No. 7, pp. 1132-1152, (2022).

[45] Z. Wang, B. Fu, Y. Wang, T. Dong, J. Li, G. Li, X. Zhao, J. Liu and G. Zhang, "Effect of Cu content on the precipitation behaviors, mechanical and corrosion properties of As-Cast Ti-Cu alloys", *Materials.,* Vol. 15, No. 5, pp. 1696-1712, (2022).

[46] Y. Xu, J. Jiang, Z. Yang, Q. Zhao, Y. Chen and Y. Zhao, "The effect of copper content on the mechanical and tribological properties of hypo-, hyper- and eutectoid Ti-Cu alloys", *Materials.*, Vol. 13, No. 15, pp. 3411-3423, (2020).

[47] J.W. Sim, J.H. Kim, C.H. Park, J.K. Hong, J.T. Yeom and S.W. Lee, "Effect of phase conditions on tensile and

antibacterial properties of Ti-Cu alloys with Ti$_2$Cu intermetallic compound", *J. Alloys Compd.,* Vol. 926, No. 12, pp. 166170-166823, (2022).

[48] Y. Yuan, R. Luo, J. Ren, L. Zhang, Y. Jiang and Z. He, "Design of a new Ti-Mo-Cu alloy with excellent mechanical and antibacterial properties as implant materials", *Mater. Lett.*, Vol. 306, No.1, pp. 130875-130927, (2022).

[49] L. Raganya, N. Moshokoa, R. Machakha, B. Obadele and M. Makhatha, "Microstructure and tensile properties of heat-treated Ti-Mo alloys", *MATEC Web of Conferences*, Vol. 370, No. 20, pp. 1-10, (2022).

[50] J. Li, X. Zang, W. Zhao, and X. Zhang, "Vacancy expansion in alpha-Ti under tensile loads at different strain rates with MD simulation", *JME.,* Vol. 7, No. 2, pp. 96-106, (2019).

[51] H.V. Swygenhoven, M. Spaczer, A. Caro and D. Farkas, "Competing plastic deformation mechanisms in nanophase metals", *Phys. Rev. B*, Vol. 60, No. 1, pp. 22–25, (1999).

[52] R. Mohammdzadeh, "Analysis of plastic strain-enhanced diffusivitycin nanocrystalline iron by atomistic simulation", *J. Appl. Phys..* Vol 125, No. 3, pp. 135103, (2019).

[53] E.H.A.N. Ma'rifah, A. Supriyanto, T. Paramitha, H. Widiyandari, A. Purwanto, H.K.K. Aliwarga, "Titanium dioxide (TiO$_2$) doping copper (Cu) with annealing temperature variation as photoanode for dye-sensitized solar cells (DSSC)", Vol. 465, No. 4, pp. 1-7, (2023).

[54] M. Jafari, A. Jahandoost, M. Vaezzadeh and N. Zarifi, "Effect of pressure on the electronic structure of hcp Titanium", *Condens. Matter Phys*., Vol. 14, No. 2, pp. 1-7, (2011).

[55] M. Jafari, "Electronic Properties of Titanium using density functional theory. *Iranian Journal of Science and Technology. Transaction A, Science*., Vol. 36, No. 4, pp. 511-515 , (2012).

[56] H.C. Wu, A. Kumar, J. Wang, X.F. Bi, C.N. Tome, Z. Zhang and S.X. Mao, "Rolling-induced face centered cubic titanium in hexagonal close packed titanium at room temperature", *Sci Rep.,* Vol. 6, No. 4, pp. 24370-24378, (2016).

**Links of all references**

1. https://doi.org/10.1038/s41578-020-0212-2
2. https://doi.org/10.1016/j.nanoms.2020.04.002
3. https://doi.org/10.1002/pol.1988.140260910
4. https://doi.org/10.12998%2Fwjcc.v3.i1.52
5. https://doi.org/10.1201/9781315368429
6. https://doi.org/10.1016/j.jmps.2017.04.005
7. https://doi.org/10.1016/j.pmatsci.2022.100933
8. https://doi.org/10.1103/PhysRev.159.98
9. https://doi.org/10.1016/j.commatsci.2018.05.030
10. https://doi.org/10.1016/j.commatsci.2017.01.002
11. https://doi.org/10.1016/j.commatsci.2017.09.039
12. https://doi.org/10.1063/1.4964654
13. https://doi.org/10.1021/acsomega.3c07561
14. https://doi.org/10.3390/app12094437
15. https://doi.org/10.3390/app12030946
16. https://doi.org/10.55713/jmmm.v34i1.1813
17. https://doi.org/10.3390/jcs6120383
18. https://doi.org/10.1016/j.mtcomm.2023.107119
19. https://doi.org/10.3390/jcs5010018
20. https://doi.org/10.3390/app12178473
21. https://doi.org/10.3390/mi14051081
22. https://doi.org/10.1007/s13632-012-0045-5
23. https://doi.org/10.3390/met11111760
24. https://doi.org/10.1557/s43579-023-00333-6

25. http://dx.doi.org/10.1007/s11665-021-06270-6

26. https://doi.org/10.3389/fmats.2020.602567

27. https://doi.org/10.1063/1.5086903

28. http://dx.doi.org/10.1088/2053-1591/ac0734

29. https://doi.org/10.1007/s11431-019-9530-6

30. https://doi.org/10.1016/j.jallcom.2019.152142

31. http://dx.doi.org/10.1016/j.commatsci.2020.109627

32. https://doi.org/10.1016/C2017-0-04711-0

33. https://doi.org/10.1016/j.commatsci.2020.109968

34. https://www.mv.helsinki.fi/home/knordlun/moldyn/lecture01.pdf

35. https://www.osti.gov/servlets/purl/1268160

36. https://doi.org/10.1080/00268978400101201

37. https://doi.org/10.1103/PhysRevA.31.1695

38. https://doi.org/10.1088/0965-0393/15/7/001

39. https://doi.org/10.1016/j.jmps.2007.11.012

40. https://doi.org/10.1103/PhysRevB.73.054104

41. https://doi.org/10.1103/PhysRevB.58.11085

42. https://doi.org/10.3390/ma16093591

43. https://doi.org/10.1016/j.ijfatigue.2017.12.010

44. https://doi.org/10.3390/met12071132

45. https://doi.org/10.3390/ma15051696

46. https://doi.org/10.3390/ma13153411

47. https://doi.org/10.1016/j.jallcom.2022.166823

48. https://doi.org/10.1016/j.matlet.2021.130875

49. https://doi.org/10.1051/matecconf/202237003007

50. https://doi.org/10.21595/jme.2019.20629

51. https://doi.org/10.1103/PhysRevB.60.22

52. https://doi.org/10.1063/1.5085659

53. https://doi.org/10.1051/e3sconf/202346502065

54. http://dx.doi.org/10.5488/CMP.14.23601

55. https://doi.org/10.22099/IJSTS.2012.2114

56. https://doi.org/10.1038/srep24370